Hindawi
Advances in Civil Engineering
Volume 2024, Article ID 3387744, 12 pages
https://doi.org/10.1155/2024/3387744

Research Article

Assessment of Ultimate Bearing Capacity of Static Loading Pile Based on Cusp Catastrophe Theory

Jibao Yang,[1] Xing Huang,[1] Hao Ni,[1] Shilong Hao,[1] Fudong Liu,[1] and Zhangrong Liu[2]

[1]*Shanghai Municipal Engineering Design Institute (Group) Co., Ltd., Shanghai 200092, China*
[2]*Department of Geotechnical Engineering, College of Civil Engineering, Tongji University, Shanghai 200092, China*

Correspondence should be addressed to Zhangrong Liu; liuzr@tongji.edu.cn

Received 26 October 2023; Revised 1 February 2024; Accepted 12 February 2024; Published 26 February 2024

Academic Editor: Chu Zhaofei

Determining the ultimate bearing capacity of pile is important for reasonable design of the pile. In this paper, a cusp catastrophe theory-based method was proposed for assessing the ultimate bearing capacity of static loading pile. Firstly, a three-parameter quartic polynomial in accordance with the standard form of cusp catastrophe model is proposed and used to fit the experimentally obtained *Q*–*S* curve. The parameters which allow the polynomial to produce best fitting to the *Q*–*S* curve are taken to identify the stability of the pile following a simple procedure. Then, the proposed method was verified against 10 *Q*–*S* curves obtained from field tests at Jinqiao-Meiya and Jinqiao-Chunyu areas of Shanghai. Results show that the ultimate bearing capacities of the piles identified by the proposed method were comparable to those identified by the JGJ 106-2014 standard method. Finally, it is found that the stability of the pile identified by the proposed method and the mechanical state of the pile identified by the Golden Section approach were correlated closely.

1. Introduction

Pile is commonly used where the ground is too weak to support the overlying structures or buildings. The loads of structures or buildings are transferred to the soils underlying the pile end and to the soils surrounding the pile shaft [1]. Both the pile end bearing and pile shaft friction contribute to the bearing capacity of the pile [2]. With increasing overlying loads, the pile tends to move downwards until reaching a balance between overlying loads and pile resistance. In this regard, determining the ultimate bearing capacity of pile is of great significance for reasonable design of the pile.

Static loading test is widely considered as the most reliable method for determining the ultimate bearing capacity of pile. In this test, static loads are applied to the head of a pile incrementally by means of hydraulic jack and the settlements of the pile head are monitored synchronously [3]. The test results can be presented as a load–settlement (*Q*–*S*) curve, which provides direct information for assessment of ultimate bearing capacity of the pile. According to their shapes, the *Q*–*S* curves can be divided into two types including plunging curves and progressive curves. The plunging *Q*–*S* curve contains a distinct inflection point, where the slope of the curve changes dramatically, indicating plunging failure of the pile. For such *Q*–*S* curve, the load corresponding to this inflection point is considered as the ultimate bearing capacity [4]. The progressive *Q*–*S* curve presents rather smoothly and contains no distinct inflection point. It is difficult to perceive the ultimate bearing capacity intuitively from such curves. For this scenario, many interpretation methods based on graphical construction, mathematical model and settlement limit have been proposed [5–7].

The graphical methods identify the ultimate bearing capacity by drawing tangent lines and auxiliary lines on the *Q*–*S* curve or its derivative form, e.g., lg*Q*–lg*S* and S/*Q*–*S* curves [8, 9].

The settlement limit-based methods simply taken a load on the *Q*–*S* curve or lg*Q*–lg*S* corresponding to a specific settlement as the ultimate bearing capacity. In the Chinese standard JCJ 106-2014, for example, the load corresponding to a settlement of 40 mm is suggested as the ultimate bearing capacity for piles slenderer than 800 mm, while for thicker piles the load corresponding to a settlement identical to 0.05 times of the pile diameter is selected. Other settlement

limits such as 25.4 mm also selected to determine the ultimate bearing capacity [10].

The mathematical model-based methods convert the original Q–S curve into a special line (usually a straight line) described by a simple function (usually a linear function) and relate the function parameter to the ultimate bearing capacity [11]. For instance, in the van der Veen [12] method the $\lg(1\text{-}Q/Q_{ult})$ is plotted versus settlements and the Q_{ult} which gives the curve a straight line is considered as the ultimate bearing capacity. Chin [13] plotted the Q–S curve as S/Q–S curve and taken its inverse slope as the ultimate bearing capacity.

Many researchers have attempted to make a comparison between different determining methods. Marcos et al. [5] evaluated eight different methods based on data of 152 load tests from 72 different sites and concluded that some methods underestimate while others overestimated the ultimate bearing capacity. Kodsy et al. [14] employed a comparative statistical analysis on 14 methods using data of 68 load tests conducted on large-diameter open-ended piles. It was concluded that none of these methods was superior to the others, and their performance was somewhat correlated. Mahmood et al. [15] compared eight commonly used methods and recognized the Debeer intersection load and Mazurkiewicz methods as the most suitable and reliable pile capacity interpretation methods for bored piles. Although different methods with unique assumptions have been proposed previously, many of the graphical methods involve qualitative analysis such as using manual manipulation to confirm the point of maximum curvature or draw tangent lines on a Q–S curve. In this case, different results can be obtained by different researchers. The settlement limit-based methods simply relate the ultimate bearing capacity to an experiential settlement without scientific demonstration.

The object of this paper is to develop a new assessment method for ultimate bearing capacity of static loading pile based on cusp catastrophe theory. Firstly, the cusp catastrophe theory was introduced briefly and related to the settlement behavior of static loading pile. Then, the performances of the new method were comparatively verified with the standard method by various Q–S curves from field tests at Shanghai. Finally, the applicability and limitations of the new method was discussed with consideration to its unique features.

2. Cusp Catastrophe Theory

In fact, as mentioned earlier, the shape of the Q–S curve can imply the state of the pile. A plunging curve with a distinct inflection point indicates plunging failure of the pile, just as a "catastrophic" phenomenon, which can be appropriately describe using cusp catastrophe theory. Whereas it is difficult to "read" the pile state directly from a progressive curve, to judge the pile state based on the cusp catastrophe theory should be an interesting attempt.

The catastrophe theory was proposed by Thom [16] in the 1970s to deal with problems of discontinuity and sudden change without insight into internal mechanisms. According to the catastrophe theory, the potential of a system is cogoverned by state variables and control variables. When no more than two state variables and no more than four control variables are involved in a system, usually seven elementary catastrophes may be observed in the system, including fold, cusp, swallowtail, butterfly, hyperbolic umbilic, elliptic umbilic, and parabolic umbilic catastrophes. The cusp catastrophe model, which contains only one state variables and two control variables, is the most simple and elementary catastrophe model and commonly used to explain various natural and engineering problems [17]. Other catastrophe models contain more variables and are more complicated for application purpose. For the static loading pile, bearing performance is the only state variable. The factors affecting the bearing performance of the pile can be sorted into two categories: properties (density, gradation, texture, etc.) of the soil and features (diameter, roughness, etc.) of the pile. Therefore, the stability of static loading pile can be described by the cusp catastrophe model.

In the cusp catastrophe model [16, 17], the standard potential function of the system is expressed as:

$$V(x) = x^4 + ux^2 + vx, \tag{1}$$

where V is the potential of the system; x is the state variable of the system; and u and v are the major and minor control variables of the system, respectively.

According to the cusp catastrophe theory, the system reaches an equilibrium state in case of zero potential gradient, i.e.,

$$\frac{\mathrm{d}V(x)}{\mathrm{d}x} = 4x^3 + 2ux + v = 0. \tag{2}$$

The geometry of the Equation (2) is called the equilibrium surface of the system. As shown in Figure 1, the equilibrium surface is a catastrophe manifold illustrating the relationship of state variable and control variables. It can be divided into upper stable region and lower stable region. In the region of $u > 0$, the upper and lower stable regions are connected continuously without fold. Otherwise in the region of $u < 0$, with the variation of the control variables, the phase trajectory of the state variable may suddenly jump from one stable region to another, resulting in the so-called catastrophe. For the static loading pile, the catastrophe corresponds to the failure of the pile under a load higher than its ultimate bearing capacity.

At the points where the catastrophe occurs, the tangent vector of the equilibrium surface is parallel to the vector of state variable (Figure 1), i.e.,

$$\frac{\mathrm{d}^2V(x)}{\mathrm{d}x^2} = 12x^2 + 2u = 0. \tag{3}$$

Equation (3) is the singularity equation of the system, indicating the condition of catastrophe for the equilibrium surface. Therefore, for a given system, the catastrophe

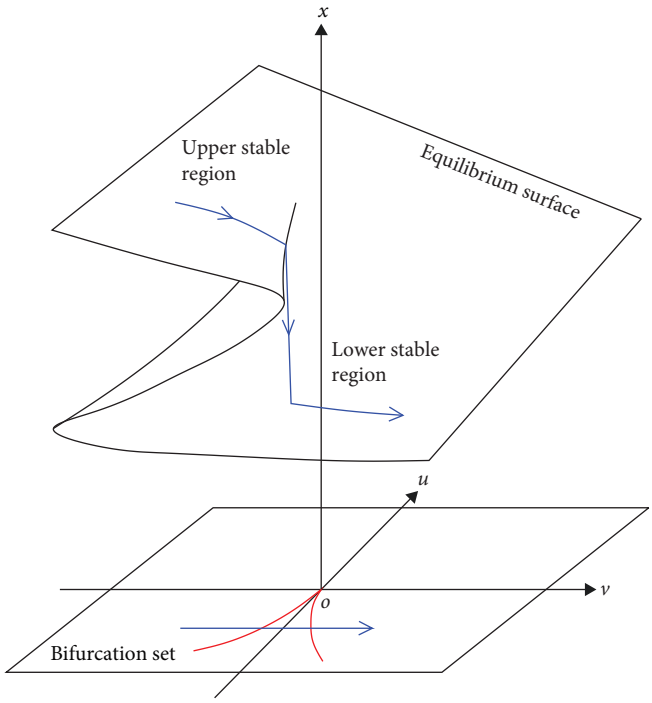

FIGURE 1: The equilibrium surface and bifurcation set of the cusp catastrophe model.

points should satisfy both the equilibrium surface equation and singularity equation. By connecting Equation (2) and Equation (3), an equation governed solely by control variables can be obtained:

$$D = 8u^3 + 27v^2 = 0. \tag{4}$$

The geometry of Equation (4) is two curves on the u–v plane (Figure 1). It looks that the u-axis bifurcate at the origin of the coordinate ($u = 0$, $v = 0$) into two branches, which grow into the third ($u < 0$, $v < 0$) and fourth ($u < 0$, $v > 0$) quadrants of the u–v plane, respectively. Therefore, the two curves are also called the bifurcation set and Equation (4) is termed as bifurcation set equation of the system. The bifurcation set has a cusp at the origin of the coordinate ($u = 0$, $v = 0$), giving rise to the appellation of cusp catastrophe. Once the phase trajectory of control variables crosses the bifurcation set (Figure 1), the state variable changes abruptly, indicating a cusp catastrophe. In the region enclosed by the bifurcation set, since $u < 0$ and v^2 is smaller than that on the bifurcation set, it is not difficult to conclude that $D < 0$, corresponding to an unstable state of the system. In contrast, there is $D > 0$ in the region outside the bifurcation set, corresponding to a stable state of the system.

3. Development of the New Method

According the cusp catastrophe theory, in order to identify the stability of a system, it is critical to establish an appropriate potential function and judge the value of the discriminant index, D. For the static loading pile, the Q–S curve reflects the stability of the pile. Straightforwardly, the curve can be described using a three-parameter quartic polynomial similar to the standard form of cusp catastrophe model:

$$S = aQ^4 + bQ^2 + cQ, \tag{5}$$

where S and Q are the settlement and load of the pile head, respectively. a, b, and c are nonzero parameters governing the shape of the curve.

If there is $a > 0$, by letting $aQ^4 = x^4$, Equation (5) can be converted into a new polynomial in accordance with the standard form of cusp catastrophe model:

$$S = x^4 + ba^{-0.5}x^2 + ca^{-0.25}x. \tag{6}$$

According to the cusp catastrophe theory, the settlement S corresponds to the potential function of the pile, which is governed by a state variable x and two control variables:

$$u = ba^{-0.5} \text{ and } v = ca^{-0.25} \tag{7}$$

According to Equation (4), the stability of the pile can be judged through the value of the discriminant index:

$$D = 8b^3a^{-1.5} + 27c^2a^{-0.5}. \tag{8}$$

When there is $D > 0$, the pile is in stable state and the current load is lower than the ultimate bearing capacity. Oppositely, when there is $D < 0$, the pile is in unstable state and the current load is higher than the ultimate bearing capacity.

If there is $a < 0$, however, the above substitution $aQ^4 = x^4$ is inapplicable. Alternatively, multiply both sides of Equation (5) by -1 and let $-aQ^4 = x^4$, Equation (5) can be converted into a new polynomial in accordance with the standard form of cusp catastrophe model:

$$-S = x^4 - b(-a)^{-0.5}x^2 - c(-a)^{-0.25}x. \tag{9}$$

Following a similar procedure described in Section 2, the discriminant index of the negative system ($-S$) can be deduced:

$$D = -8b^3(-a)^{-1.5} + 27c^2(-a)^{-0.5}. \tag{10}$$

When there is $D < 0$, the pile is in stable state and the current load is lower than the ultimate bearing capacity. Oppositely, when there is $D > 0$, the pile is in unstable state and the current load is higher than the ultimate bearing capacity.

In field tests, static loads are applied to the head of a pile step by step until plunging failure of the pile or a target settlement of the pile. After each step of loading, the stability of the pile can be evaluated according to the Q–S curve obtained at the current load level. A flow chart illustrating the assessment process of the ultimate bearing capacity using the newly proposed method is shown in Figure 2. For a given Q–S curve obtained at i^{th} step of load (Q_i), the values of

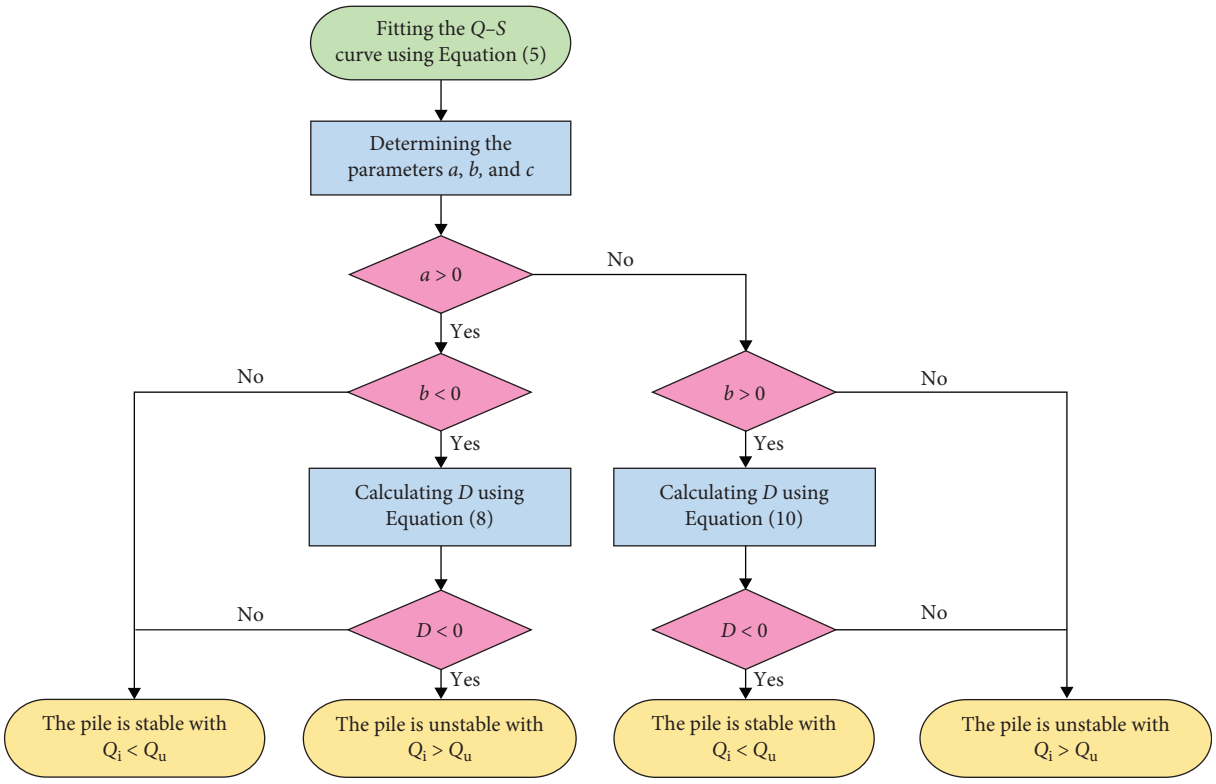

Figure 2: Assessment process of the ultimate bearing capacity using the new method.

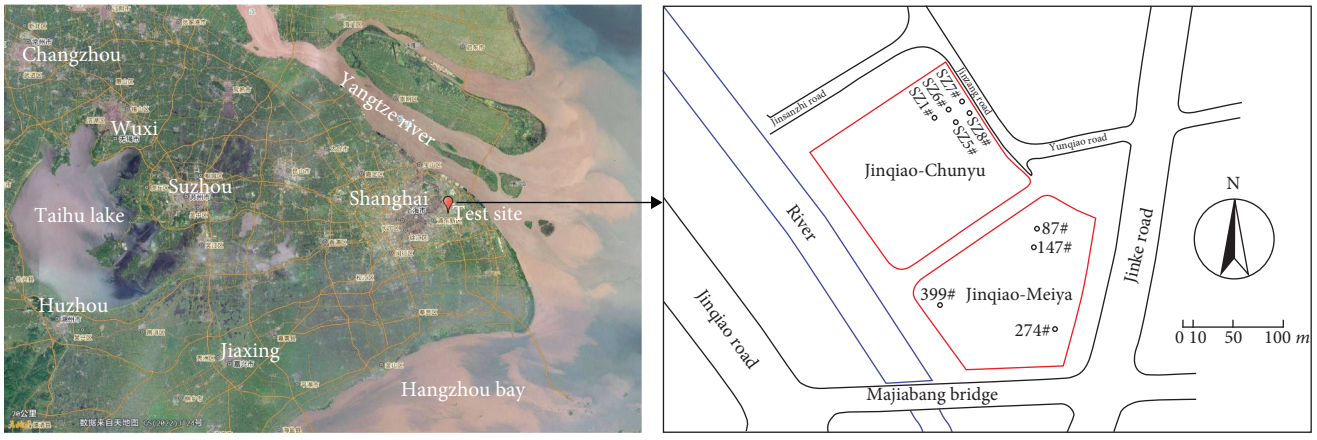

Figure 3: Schematic diagram of the location of the test site and layout of piles.

parameters a, b, and c are determined by best-fitting the curve with the Equation (5). As shown in Figure 2, if there is $a > 0$ and $b > 0$, the pile should be in stable state since there must be $D > 0$ according to the Equation (8). Obviously, in this case the current load (Q_i) is smaller than the ultimate bearing capacity (Q_u) of the pile. If there is $a < 0$ and $b < 0$, the pile should be in unstable state since there must be $D > 0$ according to the Equation (10). In other words, in this case the current load is higher than the ultimate bearing capacity of the pile. Else if there is $a > 0$ and $b < 0$, or $a < 0$ and $b > 0$, the state of the pile depends on the value of D calculated from the Equation (8) or Equation (10). For $a > 0$ and $b < 0$, the pile is stable if the D is positive. For $a < 0$ and $b > 0$, the pile is stable if the D is negative. Otherwise, the pile is unstable with load higher than its ultimate bearing capacity.

4. Verification of the New Method

In order to verify the reliability of the method proposed in this work, 10 Q–S curves obtained from field tests at Jinqiao-Meiya and Jinqiao-Chunyu areas of Shanghai were taken into account.

4.1. Field Tests. Jinqiao-Meiya and Jinqiao-Chunyu are two adjacent sites selected for constructing high-rise buildings in Pudong New Area, Shanghai, China (Figure 3). The geological

Table 1: Stratum lithology revealed by drilling hole SZ1 at Jinqiao-Chunyu site.

Layer order	Soil name	Thickness (m)	Depth (m)	Angle of internal friction (°)	Diameter of the cast-in-place pile (mm)
①$_1$	Miscellaneous fill soil	2.3	2.3	10	1,010
②	Silty clay	0.7	3.0	19.5	1,010
③$_1$	Muddy silty clay	6.0	9.0	11.4	1,010
④$_1$	Muddy clay	9.0	18.0	11.5	1,010
⑤$_{11}$	Clay	4.0	22.0	14.3	1,010
⑤$_{12}$	Silty clay	3.5	25.5	17.4	1,030
⑥	Silty clay	7.5	33.0	16.2	1,030
⑦$_{11}$	Sandy silt	2.0	35.0	30.6	1,000
⑦$_{12}$	Silt	7.5	42.5	32.7	1,080
⑦$_2$	Silt	25.5	68.0	33.7	1,030
⑨$_{11}$	Sandy silt	10.0	78.0	32.7	1,010
⑨$_2$	Medium-coarse sand	8.6	86.6	36.3	1,000

conditions of the two sites are simple and comparable, without significant fluctuations. As an example, the stratum lithology revealed by drilling hole SZ1 at Jinqiao-Chunyu site are listed in Table 1. It shows that the underground soils within 86.6 m depth can be divided into nine layers with some sublayers. Soils within 33 m depth are clays or silty clays with weak strength while those deeper are silts or sands with higher strength.

A cluster of cast-in-place piles with different diameters, lengths, and postgrouting methods were constructed and subjected to postgrouting and static loading tests at the two sites. The postgrouting was carried out at least 2 days after the complete of the cast-in-place piles to strengthen the piles, and the static loading tests followed at least 20 days later than the postgrouting to detect the bearing behavior of the piles (Figure 4). Here, 10 of these pilot piles are selected for analysis (Table 2). At the Jinqiao-Meiya site, four piles (87#, 147#, 274#, and 399#) were constructed to a designed diameter of 700 mm and a length of 65 m and then enhanced by joint end-side (E-S) postgrouting method, which means slurries were grouted from both the pile end and side to surrounding gaps and soil pores. At the Jinqiao-Chunyu site, one pile (SZ1#) with a designed diameter of 1,000 mm and a length of 86.6 m was cast-in-place and then enhanced using the E-S method. The other five cast-in-place piles had a diameter of 850 mm and a length of 67.7 m, while two of them (SZ5# and SZ6#) were strengthen using the end (E) postgrouting method, which injects slurries only through the end of the pile. After construction, the diameters at different cross-sections of each pile were measured and the maximum, minimum, and average diameters were calculated (Table 2). As expected, all the 10 cast-in-place piles were nonisodiametric with certain discrepancies between designed and measured diameters, the latter even vary considerably from depth to depth. This could be resulted from the uncontrolled flow of the postgrouting slurries and the different properties of soils at different depths. This diameter variation could influence the quality and thus the bearing capacity of the pile.

Loads (Q) were applied step by step to the head of the pile using four hydraulic jacks. For each load at 5, 15, 30, 45, 60, and further every 30 min, the settlements (S) of the pile head were monitored using four displacement sensors installed on the pile side in four orthogonal directions. When the settlement rate was equal to or smaller than 0.1 mm/hr, the load was increased to the next level. The above process was repeated until one of the following situations occurs [4]: (i) The settlement under current load level was larger than five times the settlement under the previous load level, indicating plunging failure of the pile; (ii) the settlement under current load level was larger than two times the settlement under the previous load level and still continued to increase even after 24 hr; (iii) the pile was damaged obviously; (iv) for progressive Q–S curves, the total settlement was approaching to 100 mm; and (v) the load reached the designed maximum level.

4.2. Assessment of the Ultimate Bearing Capacity. With the obtained Q–S curves, the ultimate bearing capacity of each pile are analyzed using both the JGJ 106-2014 standard method [4] and the newly proposed method (Figure 5). Briefly, in the JGJ 106-2014 standard the ultimate bearing capacity is recognized as the load when the settlement turns to increase abruptly (for plunging Q–S curves) or the load corresponding to a 40 mm settlement (for progressive Q–S curves) [4]. For piles with diameters (d) larger than 800 mm, the ultimate bearing capacity can be recognized as the load corresponding to the 0.05 d. If the settlement was larger than 40 mm, the compression of the pile should be taken into account. However, in this study this compression is ignored for simplification purpose.

The final stability and ultimate bearing capacity (Q_u) of each pile identified by both the JGJ 106-2014 standard method [4] and the proposed method are listed in Table 3. The rebound rate (R) indicates the ratio between the rebound displacement after complete unloading and the settlement at maximum loading. Overall, the ultimate bearing capacity identified by the proposed method are identical or slightly higher than that identified by the JGJ 106-2014 standard method [4]. The reason is that the proposed method takes the load previous to the load causing unstable state as the ultimate bearing capacity, regardless of the type (plunging or progressive) of the Q–S curve. For example, pile 87# was unstable at load level $Q8$ and so its previous load level $Q7$

Figure 4: Photos of the field trials at the Jinqiao-Chunyu site: (a) construction of a cast-in-place pile; (b) head of a cast-in-place pile; (c) postgrouting; and (d) static loading test.

Table 2: Characterizations of 10 cast-in-place piles at Jinqiao-Meiya and Jinqiao-Chunyu sites.

Site	Pile number	Designed diameter (mm)	Max./Min./Aver. diameter (mm)	Length (m)	Postgrouting method*
Jinqiao-Meiya	87#	700	920/660/784	65.5	E-S
	147#	700	840/680/748	65	E-S
	274#	700	780/700/748	68.3	E-S
	399#	700	920/700/777	68.1	E-S
Jinqiao-Chunyu	SZ1#	1,000	1080/1000/1019	86.6	E-S
	SZ5#	850	1000/850/876	67.0	E
	SZ6#	850	880/850/866	67.0	E
	SZ7#	850	920/860/879	67.0	E-S
	SZ8#	850	910/850/871	67.0	E-S
	SZ9#	850	880/850/866	67.0	E-S

*E denotes "end grouting" and E-S denotes "joint end-side grouting".

was taken as the ultimate bearing capacity. In the case that the pile kept stable state till the maximum load (e.g., pile 147#), it was reasonable to infer that the ultimate bearing capacity should be identical or higher than the maximum load. The JGJ 106-2014 standard method, however, depends on the type of the Q–S curve. For plunging curves (87#, SZ1#, and SZ1#), the JGJ 106-2014 standard method takes the load previous to the load causing unstable state as the ultimate bearing capacity, just as the proposed method does. In this case, the results judged from the two methods are identical. For progressive curves, the load corresponding to a settlement of 40 mm is suggested as the ultimate bearing capacity for piles slenderer than 800 mm, while for thicker piles the load corresponding to a settlement identical to 0.05 times of the pile diameter is selected. Usually, this selected load is small than the maximum load, which is identical or smaller than the ultimate bearing capacity inferred by the proposed method. In the JGJ 106-2014 standard method, the type of

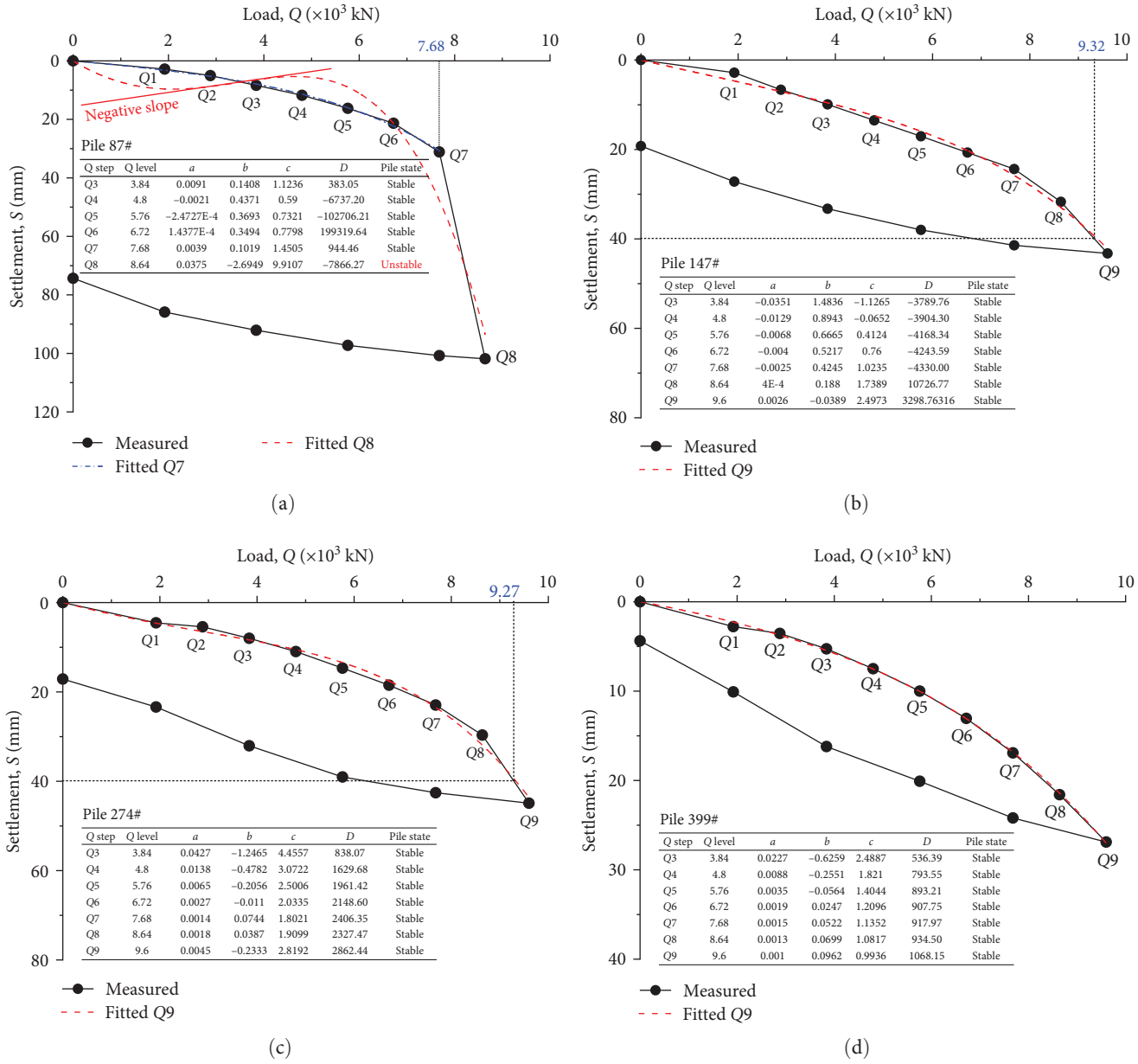

Pile 87#

Q step	Q level	a	b	c	D	Pile state
Q3	3.84	0.0091	0.1408	1.1236	383.05	Stable
Q4	4.8	−0.0021	0.4371	0.59	−6737.20	Stable
Q5	5.76	−2.4727E-4	0.3693	0.7321	−102706.21	Stable
Q6	6.72	1.4377E-4	0.3494	0.7798	199319.64	Stable
Q7	7.68	0.0039	0.1019	1.4505	944.46	Stable
Q8	8.64	0.0375	−2.6949	9.9107	−7866.27	Unstable

Pile 147#

Q step	Q level	a	b	c	D	Pile state
Q3	3.84	−0.0351	1.4836	−1.1265	−3789.76	Stable
Q4	4.8	−0.0129	0.8943	−0.0652	−3904.30	Stable
Q5	5.76	−0.0068	0.6665	0.4124	−4168.34	Stable
Q6	6.72	−0.004	0.5217	0.76	−4243.59	Stable
Q7	7.68	−0.0025	0.4245	1.0235	−4330.00	Stable
Q8	8.64	4E-4	0.188	1.7389	10726.77	Stable
Q9	9.6	0.0026	−0.0389	2.4973	3298.76316	Stable

Pile 274#

Q step	Q level	a	b	c	D	Pile state
Q3	3.84	0.0427	−1.2465	4.4557	838.07	Stable
Q4	4.8	0.0138	−0.4782	3.0722	1629.68	Stable
Q5	5.76	0.0065	−0.2056	2.5006	1961.42	Stable
Q6	6.72	0.0027	−0.011	2.0335	2148.60	Stable
Q7	7.68	0.0014	0.0744	1.8021	2406.35	Stable
Q8	8.64	0.0018	0.0387	1.9099	2327.47	Stable
Q9	9.6	0.0045	−0.2333	2.8192	2862.44	Stable

Pile 399#

Q step	Q level	a	b	c	D	Pile state
Q3	3.84	0.0227	−0.6259	2.4887	536.39	Stable
Q4	4.8	0.0088	−0.2551	1.821	793.55	Stable
Q5	5.76	0.0035	−0.0564	1.4044	893.21	Stable
Q6	6.72	0.0019	0.0247	1.2096	907.75	Stable
Q7	7.68	0.0015	0.0522	1.1352	917.97	Stable
Q8	8.64	0.0013	0.0699	1.0817	934.50	Stable
Q9	9.6	0.001	0.0962	0.9936	1068.15	Stable

Figure 5: Continued.

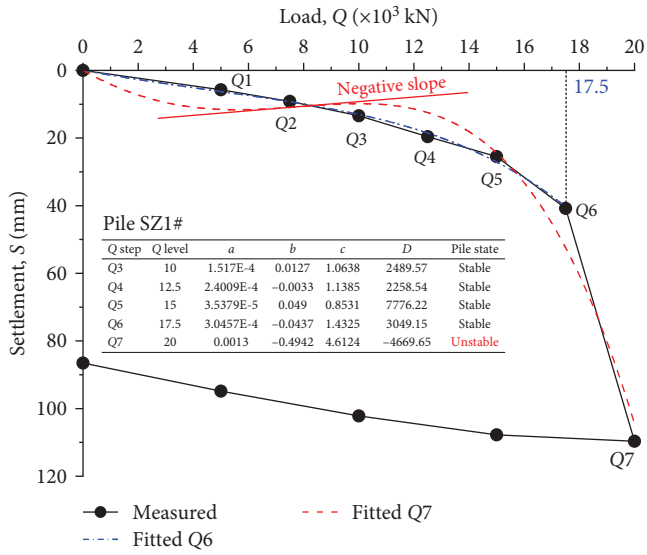

(e)

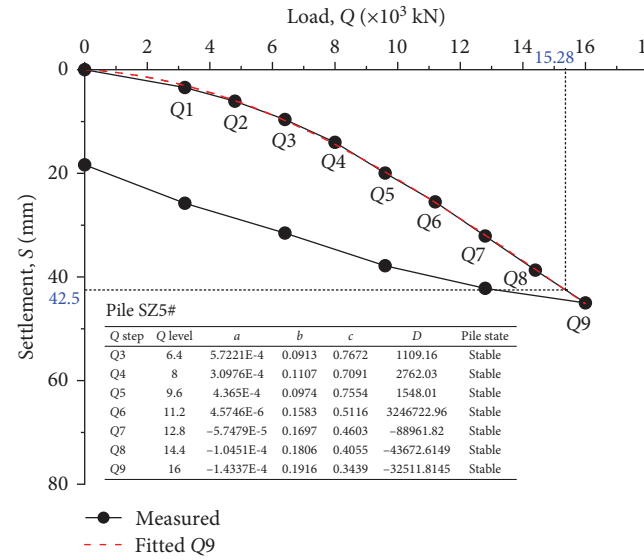

(f)

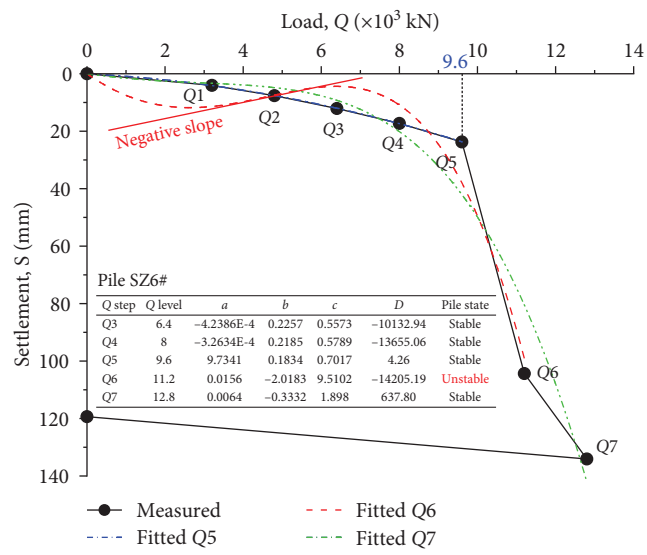

(g)

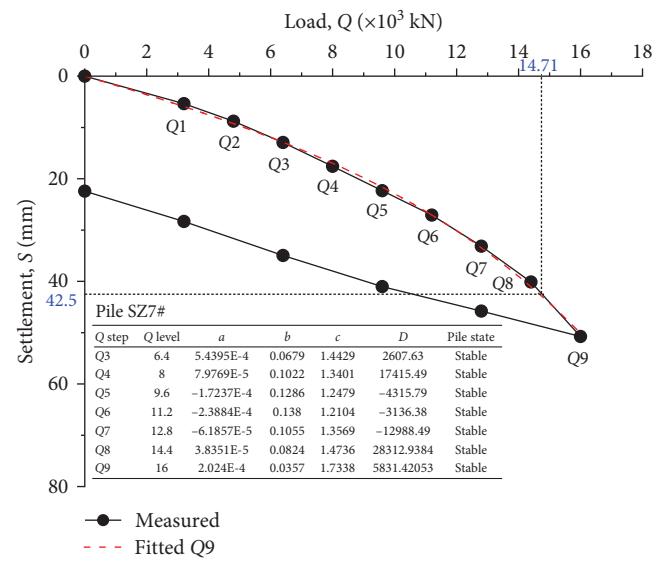

(h)

Figure 5: Continued.

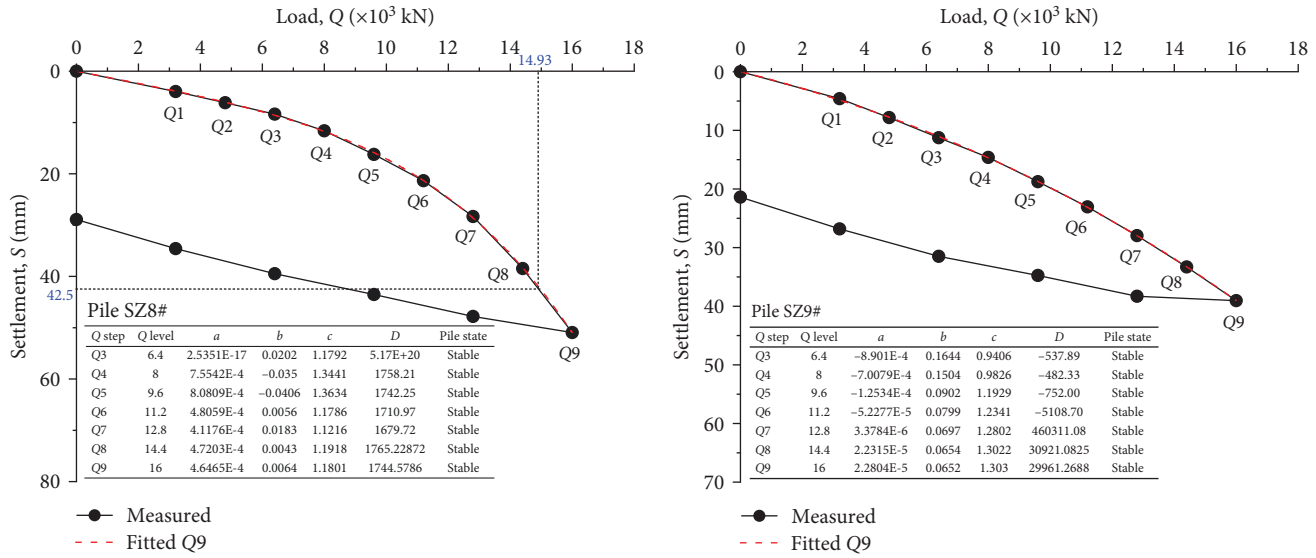

Figure 5: Analysis of Q–S curves of 10 cast-in-place piles tested at Jinqiao-Meiya and Jinqiao-Chunyu sites: (a) pile 87#, (b) pile 147#, (c) pile 274#, (d) pile 399#, (e) pile SZ1#, (f) pile SZ5#, (g) pile SZ6#, (h) pile SZ7#, (i) pile SZ8#, and (j) pile SZ9#.

Table 3: State and ultimate bearing capacity of 10 cast-in-place piles at Jinqiao-Meiya and Jinqiao-Chunyu sites.

Pile number	Q_u (JGJ 106-2014) (kN)	Q_u (Proposed) (kN)	Rebound rate	Final stability	Mechanical state
87#	7,680	7,680	27.0%	Unstable	Plastic
147#	9,320	≥9,600	55.5%	Stable	Elastic–plastic
274#	9,270	≥9,600	61.8%	Stable	Elastic
399#	≥9,600	≥9,600	83.7%	Stable	Elastic
SZ1#	17,500	17,500	21.1%	Unstable	Failed
SZ5#	15,280	≥16,000	59.2%	Stable	Elastic–plastic
SZ6#	9,600	9,600	11.0%	Stable*	Failed
SZ7#	14,710	≥16,000	55.8%	Stable	Elastic–plastic
SZ8#	14,930	≥16,000	43.2%	Stable	Elastic–plastic
SZ9#	≥16,000	≥16,000	45.2%	Stable	Elastic–plastic

*Pile SZ6# was unstable under the load previous to the final load.

the Q–S curve has to be identified visually before determining the ultimate bearing capacity. While the proposed method is straightforward without considering the type of the Q–S curve. Therefore, the proposed method can be a reliable method for practical usage.

At maximum loading, piles 87# and SZ1# are unstable with $a > 0$ and $D < 0$, while other piles are stable with $a > 0$ and $D > 0$ or $a < 0$ and $D < 0$ (Figure 5). In general, piles with larger diameters present larger ultimate bearing capacity (Table 3), thanks to larger side surface contributing more resistance to overcome pile loading. Comparing piles SZ5# and SZ6# to piles SZ7#, SZ8#, and SZ9#, it seems there is no obvious relationship between the ultimate bearing capacity and the postgrouting method. Both end-grouted and joint end-side grouted piles can be subjected to plunging failure (Figure 5). This may mean that the failure mode of the statically loading pile is mainly governed by the end-strength of the end-grouted cement paste rather than that of the joint end-side grouted one.

5. Discussion

The proposed method is capable of identifying the stability of the pile under different loads. In fact, this method is highly dependent on the shape of the Q–S curve and the distribution of test data along the curve. Taken the pile 87# as an example, as the load increases from 3,840 to 7,680 kN, the settlement of pile head increases steadily from 8.37 to 31.13 mm, without significant difference between adjacent settlement increment (Figure 5). When the load increases further to 8,640 kN, the settlement of pile head increases sharply to 101.84 mm. Meanwhile, the pile turns to unstable. Similar phenomena can be observed on piles SZ1# and SZ6# (Figure 5). The other piles keep stable till the maximum load, without significant difference between adjacent settlement increment (Figure 5). Therefore, a sharp increase of settlement indicates that the pile turns from stable to unstable state.

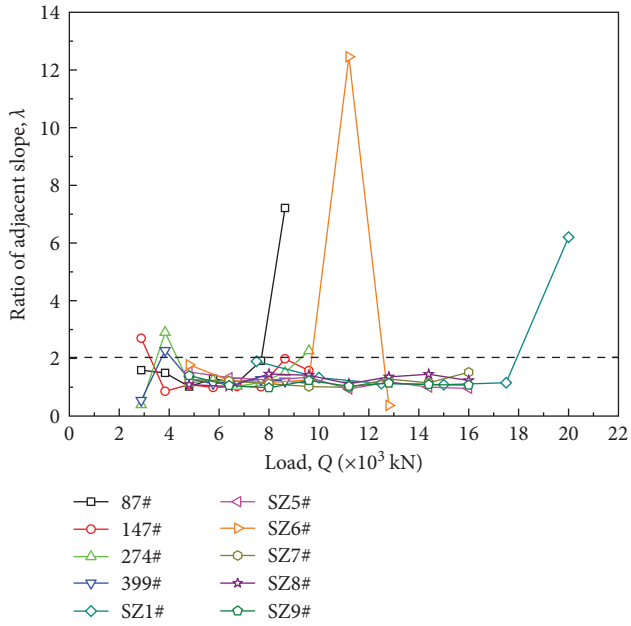

FIGURE 6: Variation of ratio of adjacent slope with load.

It is noted that for the unstable piles (87#, SZ1#, and SZ6#), the fitted Q–S curves (red dash lines in Figure 5) are twisted with negative slopes, while the fitted curves of other stable piles are monotonic with increasing slope. The negative slope indicates that the settlement decreases with the increase of load. This is obviously unreasonable. In fact, such twisted curve reflects the sudden change of the balance state of the pile. This is why the state of the pile can be evaluated by the cusp catastrophe theory.

In order to evaluate the settlement increasement with increasing load, the slope of the Q–S curve at a given loading is calculated as the ratio of settlement increasement to the load increasement, i.e.,

$$K_i = \frac{S_i - S_{i-1}}{Q_i - Q_{i-1}}, \tag{11}$$

where K_i, S_i, and Q_i are the slope, settlement, and load at the i^{th} loading, respectively. S_{i-1} and Q_{i-1} are the slope, settlement, and load at the $(i\text{-}1)^{th}$ loading, respectively. Obviously, for a given load increasement, the larger the settlement increasement, the higher the slope.

As the loading increases from $(i-1)^{th}$ to i^{th}, the slope changes from K_{i-1} to K_i. For each pile, the ratio of K_i to K_{i-1} is calculated using Equation (12) and plotted in Figure 6. The larger the λ, the steeper the Q–S curve.

$$\lambda = \frac{K_i}{K_{i-1}}, \tag{12}$$

where λ is the ratio of adjacent slope.

According to Figure 6, it seems that generally the ratio of adjacent slope (λ) is slightly larger than 1.0 and the pile is stable. For piles 87#, SZ1#, and SZ6#, the λ increases sharply to a level several times higher than 2.0 at their maximum load or submaximal load, where they are unstable as identified using the proposed method (Figure 5). The sudden increase of λ indicates the Q–S curve under present load becomes steeper comparing to that under the previous load. Such change indicates a plunging failure of the pile. In this case, there usually is $a > 0$ and $D < 0$ (Figure 5), suggesting an unstable state of the pile. Therefore, the proposed method is sensitive to plunging failure of the pile.

It is noteworthy that the pile SZ6# is unstable under 11,200 kN while turns to stable again under 12,800 kN (Figures 5 and 6). After completely unloaded, the settlement decreases from 134.10 to 119.35 mm with a rebound rate of only 11.0%. The reason could be that the end-grouted cement paste supporting the pile SZ6# was damaged under 11,200 kN loading and then compacted by the subsequent 12,800 kN loading, resulting in a sudden settlement followed by a gentle settlement of the pile. While unloading, the pile settlement rebounded insignificantly due to the end-grouted cement paste was failed without large elasticity. Therefore, for the sake of determining a reliable ultimate bearing capacity, it is also important to evaluate the mechanical state of the pile.

Depending on load level, the mechanical state of an object may be elastic, elastic–plastic, plastic, and failed. In elastic state, the strain changes linearly with the stress. In elastic–plastic and plastic state, the relationship between strain and stress is nonlinear. In failed state, the object almost loses its strength completely. The elasticity of the object, i.e., the rebound rate of the object upon unloading, decreases with object turns from elastic state to elastic–plastic, plastic, and failed state. Therefore, the mechanical state of a pile can be roughly divided into elastic, elastic–plastic, plastic, and failed state according to the rebound rate of the pile. In some previous studies, the pile state was roughly divided into linear, plastic, and failure stages according to the change trend of the Q–S curves [18]. Here, the Golden Section approach is used to identify the mechanical state of the pile.

Golden Section has been widely used as an optimization approach in solving scientific, technical, and engineering problems. By Golden Section approach, a line segment is divided into two parts in such a way that the length ratio of the longer part to the original line segment is equal to that of the shorter part to the longer part. Interestingly, this ratio should be 0.618 and known as the Golden Ratio. The line segment can be divided continuously with the Golden Section sequence (0.618^n, n is the number of dividing). Accordingly, the division of elastic, elastic–plastic, plastic, and failed state of a pile can be obtained after three times of Golden Section. As shown in Figure 7, rebound rates between 100% and 61.8%, 61.8% and 38.2% ($=(61.8\%)^2$), 38.2% and 23.6% ($=(61.8\%)^3$) as well as smaller than 23.6% are corresponding to elastic, elastic–plastic, plastic, and failed state, respectively.

According to Figure 7, the mechanical state of each pile is identified and listed in Table 3. Piles in stable state as identified using the proposed method are in elastic or elastic–plastic state, while those unstable piles are in plastic or failed state. However, the pile SZ6# is an exception. Although the pile SZ6# is stable at the maximum load, it failed under the former

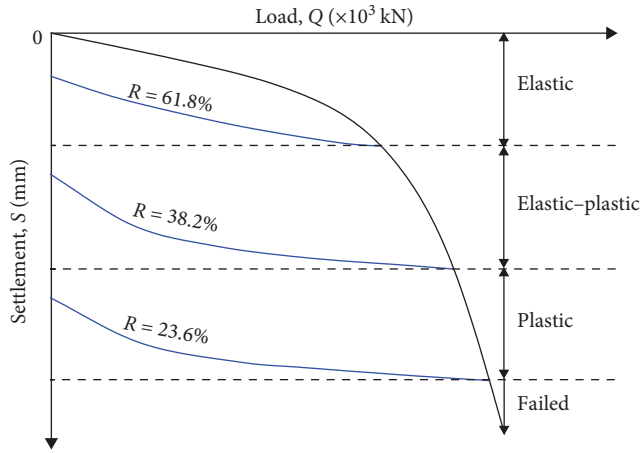

Figure 7: Division of mechanical state of the pile by Golden Section approach.

112,000 kN. Therefore, it is not contradictory to conclude that at its maximum loading the pile SZ6# is stable but in failed state.

The *Q*–*S* curves presented in this study were obtained from postgrouting strengthened cast-in-place piles established at two adjacent sites with similar stratigraphic properties. Although the *Q*–*S* curves could vary with stratigraphic property (e.g., sandy, silty, clayey, complex strata) and pile type (e.g., precast pile, friction pile, end-bearing pile), they can always be identified as either plunging or progressive types according to their shapes. As verified above, both types of *Q*–*S* curves can be satisfactorily assessed by the proposed method. Therefore, it is believed that the proposed method can be applied to other types of pile constructed at various sites. Of course, further studies on this point are expected.

6. Conclusions

In this paper, a cusp catastrophe theory-based method was proposed for assessing the ultimate bearing capacity of static loading pile. The performance of the new method was verified by various *Q*–*S* curves from field tests at Shanghai. Based on the results, the following conclusions can be obtained.

The *Q*–*S* curve of static loading pile can be satisfactorily described using a three-parameter quartic polynomial similar to the standard form of cusp catastrophe model. Accordingly, the discriminant index of the system can be calculated using the fitted parameters. The stability of the pile can be evaluated by considering both the fitted parameters and discriminant index following a simple process. The proposed method was verified against 10 *Q*–*S* curves obtained from field tests at Jinqiao-Meiya and Jinqiao-Chunyu areas of Shanghai. The ultimate bearing capacities of the piles identified by the proposed method were comparable to those identified by the JGJ 106-2014 standard method. When the pile turns to unstable state as identified by the proposed method, the ratio of adjacent slope of the *Q*–*S* curve increases sharply. To determine the ultimate bearing capacity of static loading pile, both the stability of the pile identified by the proposed method and the mechanical state of the pile identified by the Golden Section approach should be taken into account. It is found that an unstable pile corresponds to plastic or failed mechanical state.

Data Availability

Data will be made available by the corresponding author on reasonable request.

Conflicts of Interest

The authors declare that they have no conflicts of interest or personal relationships that could have appeared to influence the work reported in this paper.

Authors' Contributions

Jibao Yang contributed in the project administration, conceptualization, methodology, investigation, data curation, and writing–review & editing. Xing Huang contributed in the methodology, investigation, and data curation. Hao Ni contributed in the software and writing–review & editing. Shilong Hao contributed in the project administration and Investigation. Fudong Liu contributed in the software and data curation. Zhangrong Liu contributed in the funding acquisition, formal analysis, visualization, and writing–original draft.

Acknowledgments

The financial support from the National Natural Science Foundation of China (42002291) and the Shanghai Geological Society (Dzxh202309) are greatly acknowledged.

References

[1] C. Leblanc, G. T. Houlsby, and B. W. Byrne, "Response of stiff piles in sand to long-term cyclic lateral loading," *Géotechnique*, vol. 60, no. 2, pp. 79–90, 2010.

[2] N.-D. Hoang, X.-L. Tran, and T.-C. Huynh, "Prediction of pile bearing capacity using opposition-based differential flower pollination-optimized least squares support vector regression (ODFP-LSSVR)," *Advances in Civil Engineering*, vol. 2022, Article ID 7183700, 25 pages, 2022.

[3] ASTM D-1143/D1143M, "Standard test methods for deep foundations under static axial compressive load," 2007.

[4] JGJ 106-2014, *Technical Code for Testing of Building Foundation Piles*, China Architecture & Building Press, Beijing, 2014.

[5] M. C. M. Marcos, Y.-J. Chen, and F. H. Kulhawy, "Evaluation of compression load test interpretation criteria for driven precast concrete pile capacity," *KSCE Journal of Civil Engineering*, vol. 17, no. 5, pp. 1008–1022, 2013.

[6] N. S. Hassan, A. Ibrahim, R. Alias, D. Z. A. Hasbollah, and A. B. Ramli, "Assessment of ultimate bearing capacity of the pile for jacking & rotary piling method," *Physics and Chemistry of the Earth, Parts A/B/C*, vol. 129, Article ID 103331, 2023.

[7] H. Ma and C. Peng, "Analysis and application of ultimate bearing capacity of squeezed branch pile," *Geotechnical and Geological Engineering*, vol. 41, no. 6, pp. 3823–3828, 2023.

[8] M. Olgun, A. Hanati, and Y. Yenginar, "Evaluation of pile loading test results by different methods," in *Digital Proceeding of ICOCEE-CAPPADOCIA2017*, Nevsehir, Turkey, 2017.

[9] R. Adel and R. R. Shakir, "Evaluation of static pile load test results of ultimate bearing capacity by interpreting methods, IOP Conf," *IOP Conference Series: Earth and Environmental Science*, vol. 961, no. 1, Article ID 012013, 2022.
[10] K. Terzaghi and R. B. Peck, *Soil Mechanics in Engineering Practice*, Wiley, New York, 2nd edition, 1967.
[11] I. Vural, H. Kabaca, and S. Poyraz, "A novel approach proposal for estimation of ultimate pile bearing capacity based on pile loading test data," *Applied Sciences*, vol. 13, no. 13, Article ID 7993, 2023.
[12] C. van der Veen, "The bearing capacity of a pile," in *Proceedings of 3rd International Conference on Soil Mechanics and Foundation Engineering (Switzerland)*, vol. 2, pp. 84–90, Organizing Committee Comité d'Organisation ICOSOMEF, 1953.
[13] F. K. Chin, "Estimation of the ultimate load of piles from tests not carried to failure," in *Proceedings of Second Southeast Asian Conference on Soil Engineering*, pp. 81–90, Southeast Asian Society of Soil Engineering, 1970.
[14] A. Kodsy, N. Machairas, and M. G. Iskander, "Assessment of several interpreted pile capacity criteria for large-diameter open-ended piles," *Geotechnical Testing Journal*, vol. 44, no. 5, pp. 1217–1243, 2021.
[15] A. Mahmood, B. Alshameri, M. H. Khalid, and S. M. Jamil, "Comparative study of various interpretative methods of the pile load test," *Innovative Infrastructure Solutions*, vol. 7, Article ID 102, 2022.
[16] R. Thom, *Structural Stability and Morphogenesis: An Outline of a General Theory of Models*, pp. 1–348, CRC Press, 1975.
[17] H. Feng, Z. Wang, and P. Wei, "A novel index model for defrosting initiating time point of air source heat pump based on the cusp catastrophe theory," *Energy and Buildings*, vol. 263, Article ID 112016, 2022.
[18] M. Zhou, L. Xing, Y. Chen, and H. Qiao, "Settlement characteristics of split grouting pile composite foundation in loess areas," *Advances in Civil Engineering*, vol. 2022, Article ID 8627124, 14 pages, 2022.